Supporting information

Dual-functional Li^+ diffusion network in high nickel cathode for solid-state Li metal batteries

Meng Ye, Zhian Zhang, Jianhua Chen, Qiuyue Chen, Jiarui Hu, Lang Qiu, Fang Wan*, and Xiaodong Guo*

School of Chemical Engineering, Sichuan University, Chengdu 610065, PR China

E-mail: wanfang2022@scu.edu.cn, xiaodong2009@scu.edu.cn

Experimental methods

Preparation of GRSE electrolyte. Poly (vinylidene fluoride) (PVDF, Mw=1,000,000, Arkema, 99.9 %) and Bis(trifluoromethane)sulfonimide lithium (LiFSI, Aladdin, 99.9 %) at the mass ratio of 1:1.25 were dissolved into N, N-Dimethylformamide (DMF, Chengdu Kelong, 99.9 %). Then, $Li_{6.4}La_3Zr1.4Ta_{0.6}O_{12}$ (LLZTO, Hefei Kejing Material Technology Co., LTD, ⩽500 nm) was added into the solution and ball-milled for 12 h. The mass ratio of PVDF and LLZTO is 3:7. The slurry was then cast onto a glass substrate and dried on the vacuum oven. The dried GRSE was punched into disks with the diameter of 16 mm for further use.

Preparation of NCM@PVDF and NCM@PAN particle. PVDF and LiFSI at the mass ratio of 1:1 were dissolved in DMF, and then, $LiNi_{0.8}Co_{0.1}Mn_{0.1}O_2$ (NCM 811, Guangdong Canrd New Energy Technology Co., Ltd.,) was added into the solution and stirred for 24 h (PVDF is 2 wt% of NCM). The reaction product is dried in a vacuum oven, and the NCM@PVDF particles can be obtained. Using the same method, NCM@PAN particles can be obtained.

Preparation of cathode. NCM cathode is prepared by the following method: NCM, PVDF, LiFSI and acetylene black (Guangdong Canrd New Energy Technology Co., Ltd.) were mixed in an agate mortar under vigorous agitation at the mass ratio of 7:1:1:1, and few drops of 1-methyl-2-pyrrolidinone (NMP, Guangdong Canrd New Energy Technology Co., Ltd., 99.9 %) were added to form slurry. After that, the slurry was cast onto Al foil and dried inside a vacuum oven at 120 ℃ overnight.

NCM@PVDF and NCM@PAN cathode is prepared by the following method: NCM@PVDF or NCM@PAN, PVDF, LiFSI and acetylene black (Guangdong Canrd New Energy Technology Co., Ltd.) were mixed in an agate mortar under vigorous agitation at the mass ratio of 7.14:0.86:0.86:1, and few drops of 1-methyl-2-

pyrrolidinone (NMP, Guangdong Canrd New Energy Technology Co., Ltd., 99.9 %) were added to form slurry. After that, the slurry was cast onto Al foil and dried inside a vacuum oven at 120 ℃ overnight. The mass loading of active materials was 3-4 mg cm^{-2}.

Materials characterization. The morphology was characterized by Scanning Electron Microscopy (SEM: ZEISS GeminiSEM 300). The internal structure was characterized by Transmission Electron Microscopy (TEM: JEOL JEM-F200) and the elements distribution was analyzed by Energy Dispersive Spectrometer (TEM-EDS). The rugosity of sample surface was characterized by Sensofar integrated 3D surface optical profiler (S neox, Sensofar). The mechanical property was tested by Electronic universal testing machine (CMT 4104) at a tensile speed of 5 mm min^{-1}. Nanoindentor (Anton paar UNHT) was used to test the pressure resistance. The composition and chemical state of chemical compound were analyzed by Fourier Transform Infrared Spectrometer (FTIR: Thermo Scientific Nicolet iS5), Raman spectra (Raman WITec alpha300R) and X-ray photoelectron spectrometer (XPS: Thermo Scientific K-Alpha).

Electrochemical test. All electrochemical tests are carried out in R2032-type coin cells which were assembled in Ar-filled glovebox, and all tests were performed at room temperature. Cycling performance, rate capability, galvanostatic intermittent titration technique (GITT) and galvanostatic charge-discharge (GCD) profiles were tested by Neware battery tester (5 V, 10 mA). The linear sweep voltammetry (LSV), cyclic voltammetry (CV), leakage curves and Nyquist plots were tested by electrochemical workstation (CHI 660D).

The lithium transference number (t_{Li^+}) can be calculated by Equation (1) according to the results of Figure S5:

$$t_{Li^+} = \frac{I_s(\Delta V - I_0 R_0)}{I_0(\Delta V - I_s R_s)} \quad (1)$$

where ΔV is the polarize voltage, I_0 and I_s are the initial current and steady-state currents, respectively, and R_0 and R_s are the interfacial resistance before and after polarization, respectively.

The ionic conductivity (δ, S cm^{-1}) was calculated by the Equation (2) according to the Nyquist plots results of Figure S6:

$$\delta = \frac{d}{Re \times S} \quad (2)$$

where d (cm) is the thickness of GRSE film, Re (Ω) is the bulk resistance obtained in Figure S6, and S (cm^{-2}) is the effective area of SE||GRSE||SE cell.

The activation energy (Ea) was calculated following Equation (3) according to the δ results:

$$\delta = \delta_0 \exp(-\frac{Ea}{RT}) \quad (3)$$

where Ea (eV) is the activation energy of ion transport and δ_0 is the preexponential factor.

THEORETICAL CALCULATION

Calculation of Li$^+$ ion migration rate. The optimization of NCM811 surface (0 0 3) surface and different PVDF molecular structure effect on the solid electrolyte reactivity were studied by the First-principles method using the DMol^3 module and GGA-PW91.[1, 2] The OBS custom method was chosen for DFT-D. The convergence tolerance of the (a) maximum energy was 2x10^{-5} Ha, (b) maximum force was 0.004 Ha/ Å and (c) maximum displacement was 0.005 Å. The Li$^+$ ions migration rate of solid electrolyte was studied by the Forcite method. The dynamics of the solid electrolyte was studied with constent temperature and isopiestic pressure. The temperature was set as 298 K and pressure was 0.1 Mpa. The COMPASSII forcefield was chosen. All the charges in the system were forcefield assigned.

Calculation of Li^+ diffusion energy barriers. All calculations were performed by using the projector augmented wave method in the framework of density functional theory (DFT), as implemented in the Vienna Ab initio Simulation Package (VASP).[3] The electron exchange-correlation interactions were parameterized by the generalized gradient approximation (GGA) with the Perdew-Burke-Ernzerhof (PBE).[4, 5] Spin polarization effect was considered in this work. The Brillouin zone was sampled by the Γ-centered k-mesh with a resolution of $2\pi \times 0.04$ $Å^{-1}$ for geometry optimization. The plane-wave energy cutoff was set to 450 eV, and the convergence tolerance for residual force and energy on each atom during structure relaxation were set to 0.02 eV/Å and 10^{-5} eV, respectively. Due to strong correlation of *d*-orbital electrons of transition metal atoms, the Hubbard U correction of 6.7 eV was included in the Hamiltonian for Ni atoms based on previous studies.[6] Van der Waals interaction (DFT-D3 method with Becke-Jonson damping) was incorporated.[7, 8] Structural visualization was conducted utilizing the VESTA software.[9] The climbing-image nudged elastic band (CI-NEB) method implemented in VASP was performed to investigate the transition state searches.[10]

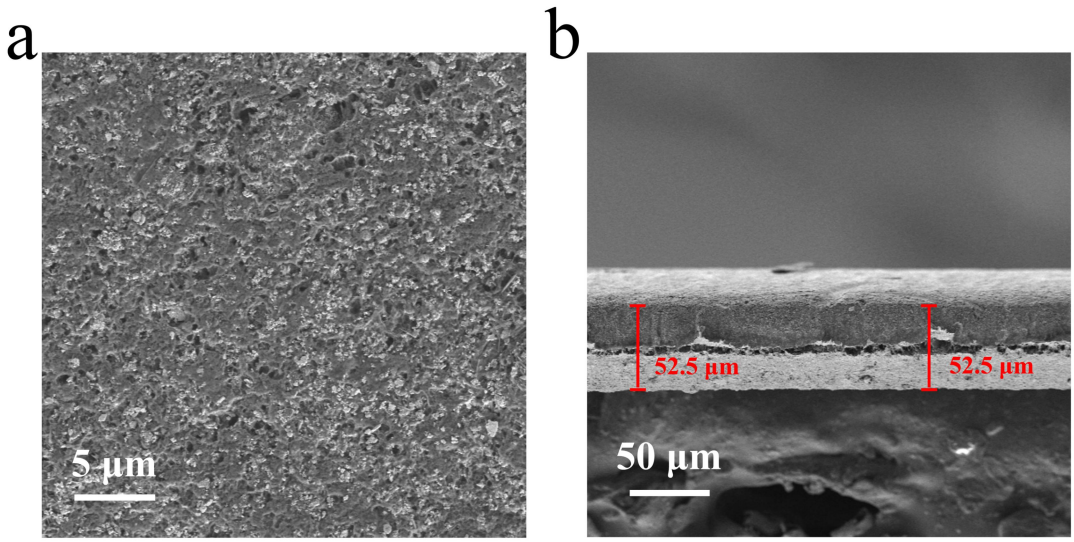

Figure S1. SEM images of (a) surface and (b) cross section of the GRSE electrolyte.

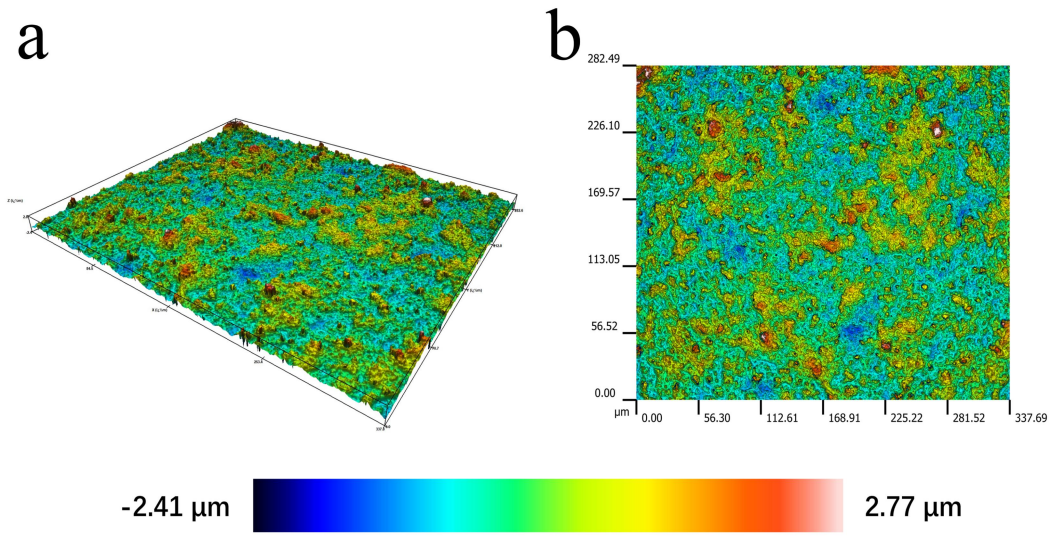

Figure S2. Optical profile images of CRSE electrolyte.

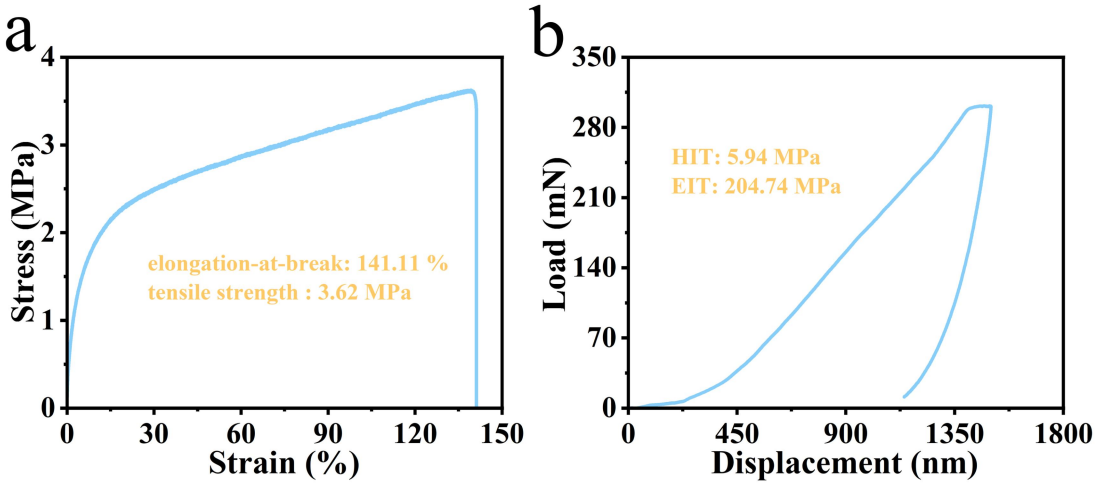

Figure S3. (a) Tensile test and (b) nanoindentation test for GRSE electrolyte.

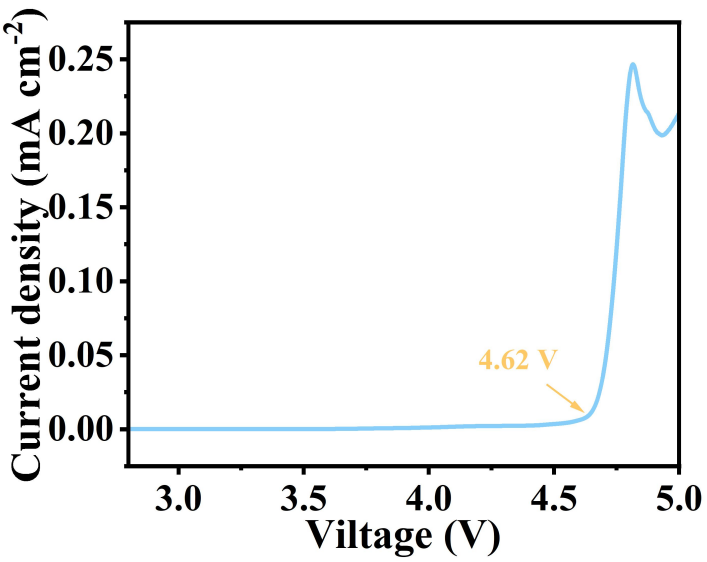

Figure S4. LSV curve of SE/GRSE/Li battery with the scan rate of 0.1 mV s^{-1}.

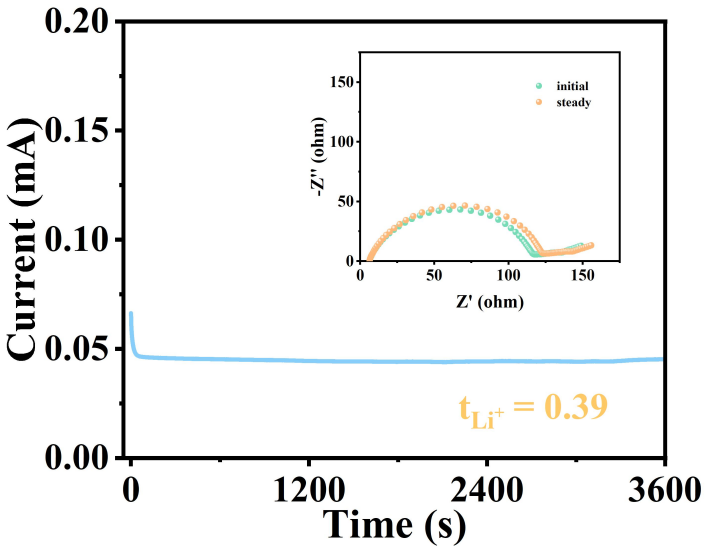

Figure S5. Variation of current with time during polarization of a Li/sample/Li battery at the voltage of 10 mV. The inset is the Nyquist plots before and after polarization.

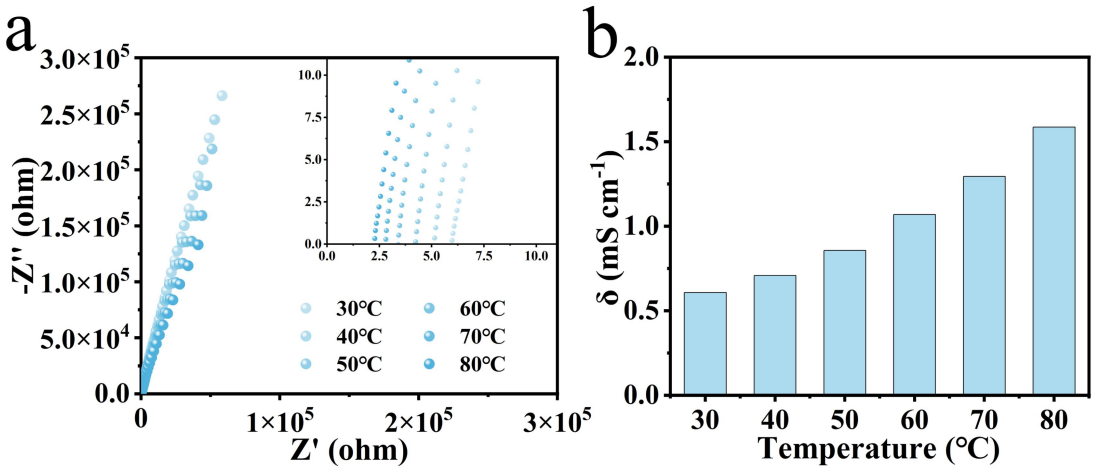

Figure S6. (a) Nyquist plots of SE/GRSE/SE battery at different temperatures. (b) The ionic conductivity of GRSE.

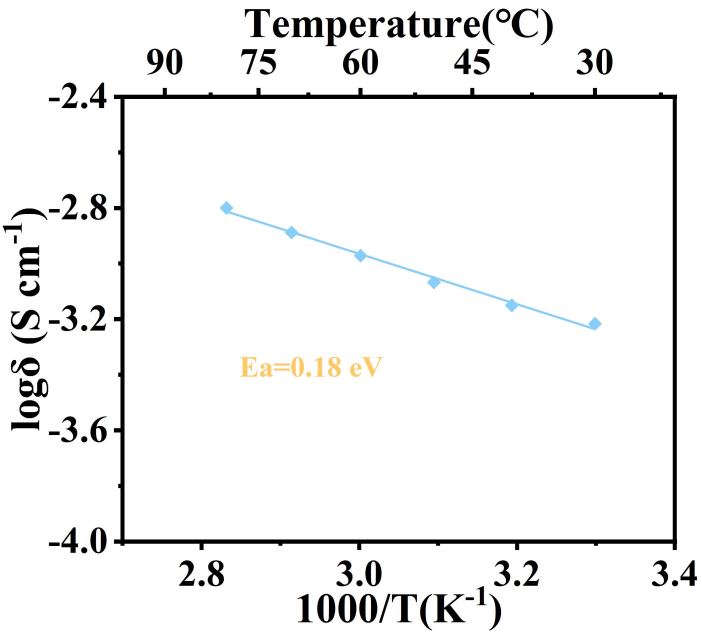

Figure S7. Arrhenius plots of the GRSE in the temperature range of 30-80 ℃.

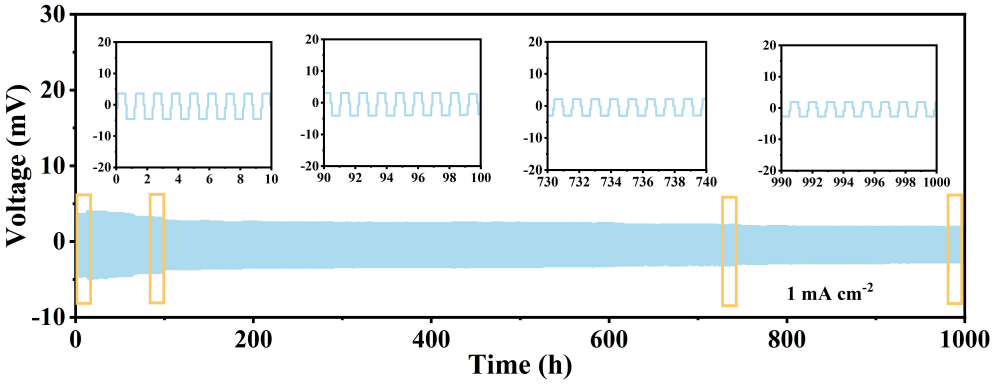

Figure S8. GCD test result of the Li/GRSE/Li battery at a current density of 0.1 mA cm^{-1}.

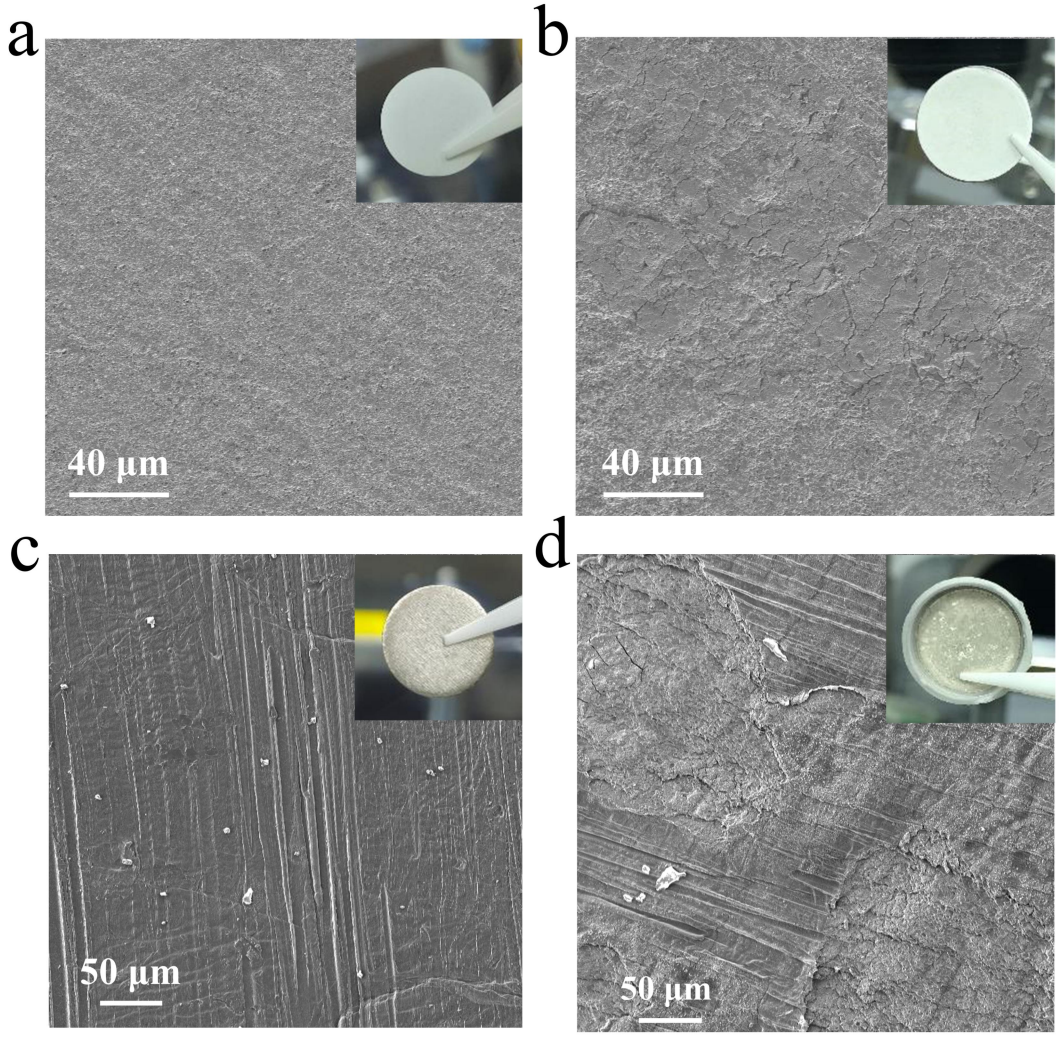

Figure S9. SEM images and the corresponding digital images of GRSE (a) before and (b) after GCD test. SEM images and the corresponding digital images of Li electrode (c) before and (d) after GCD test.

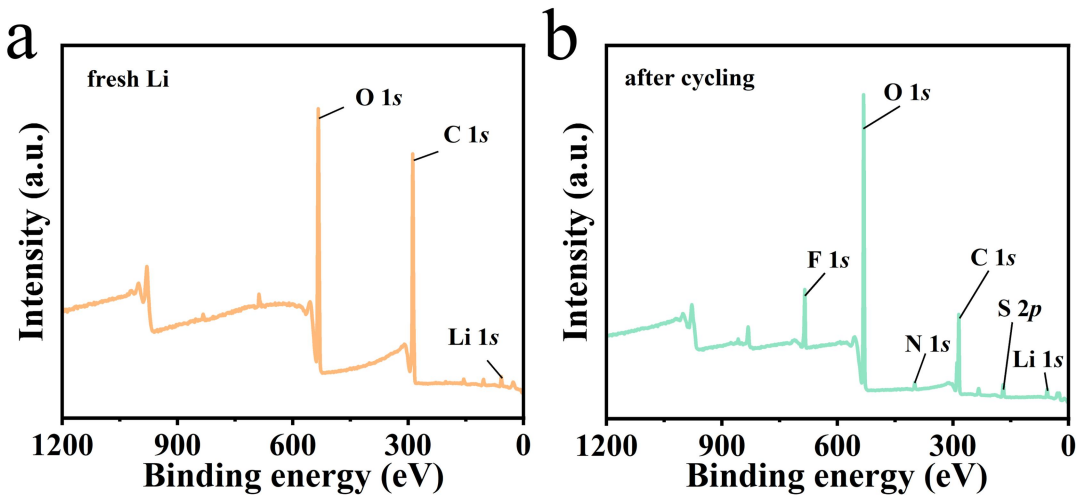

Figure S10. XPS spectra of Li electrode (a) before and (b) after GCD test.

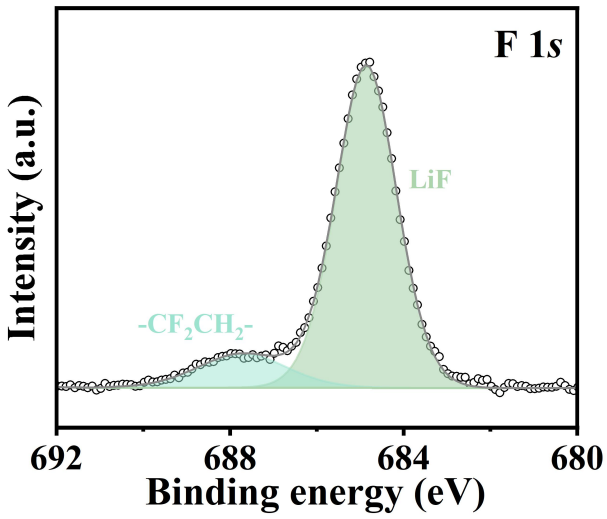

Figure S11. F 1s fine XPS spectrum of Li electrode after GCD test.

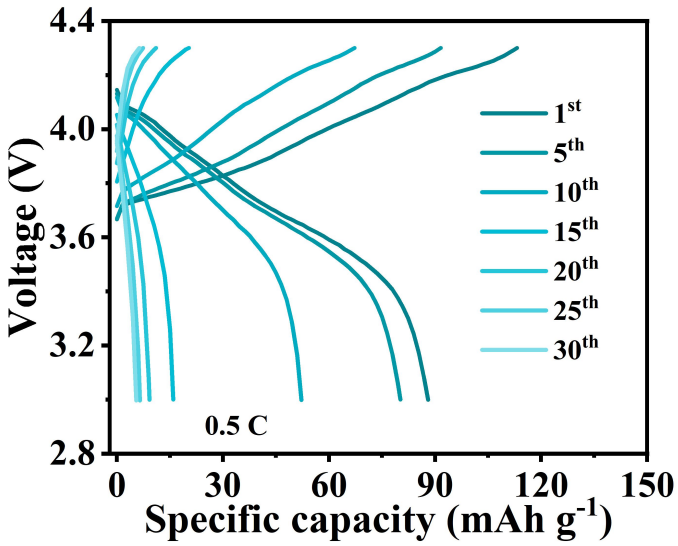

Figure S12. GCD profiles of NCM battery at 0.5 C.

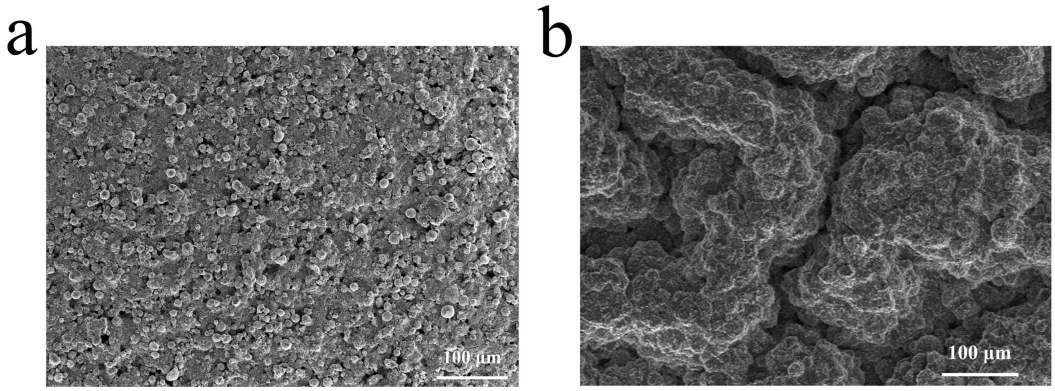

Figure S13. SEM images of NCM cathode (a) before and (b) after 50 cycles.

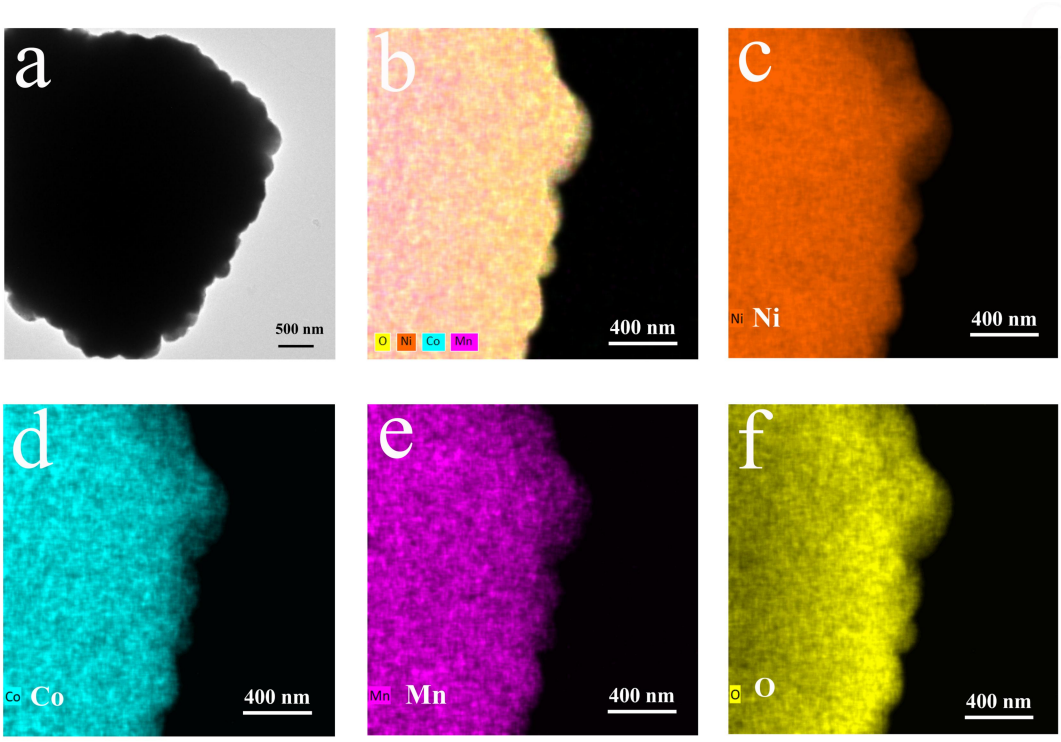

Figure S14. (a) TEM image of NCM particle. (b-f) EDS mapping images of NCM particle.

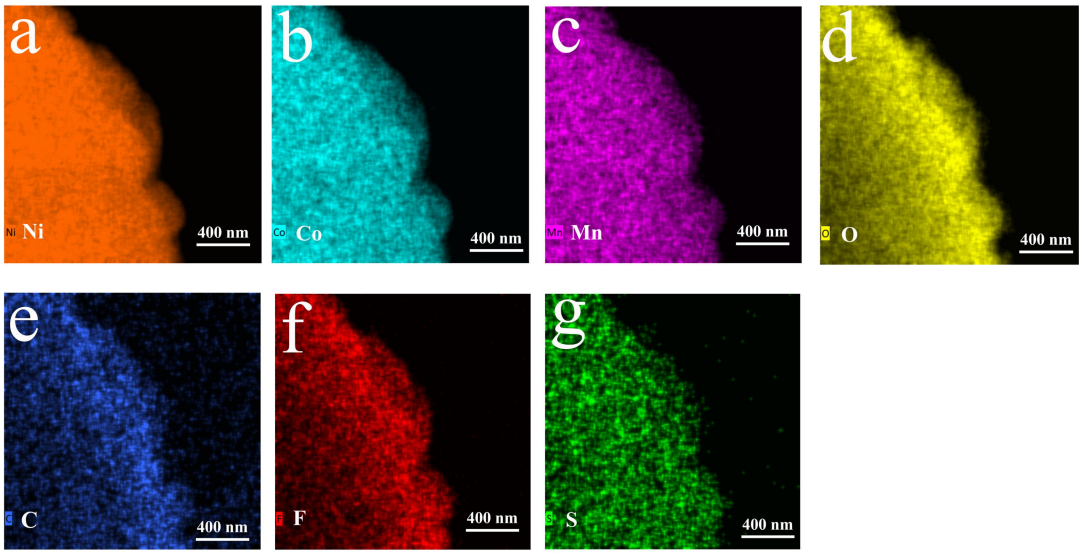

Figure S15. EDS mapping images of NCM@PVDF particle.

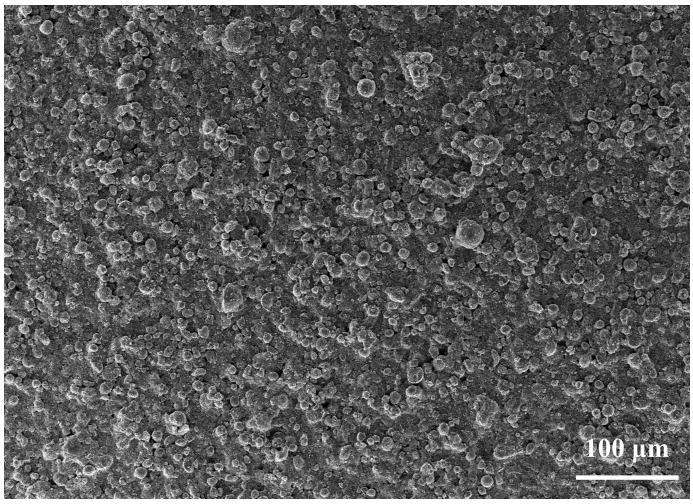

Figure S16. SEM image of the surface of NCM@PVDF cathode.

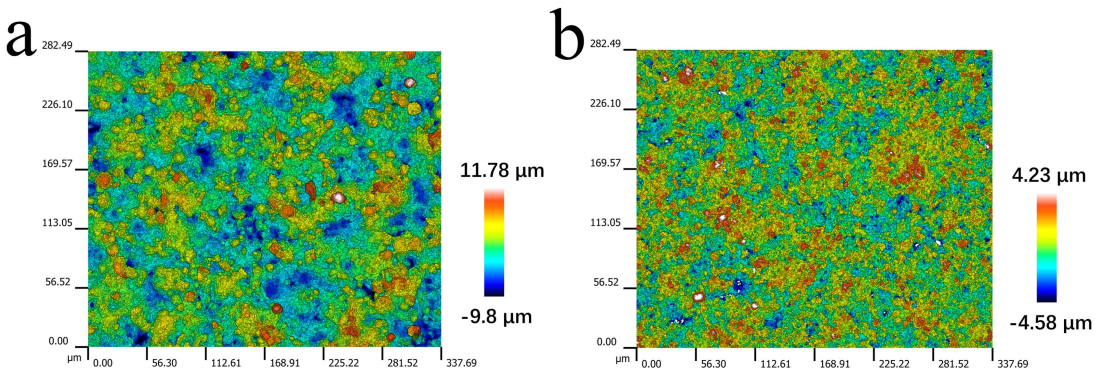

Figure S17. 2D optical profile images of NCM (a) cathode and (b) NCM@PVDF cathode.

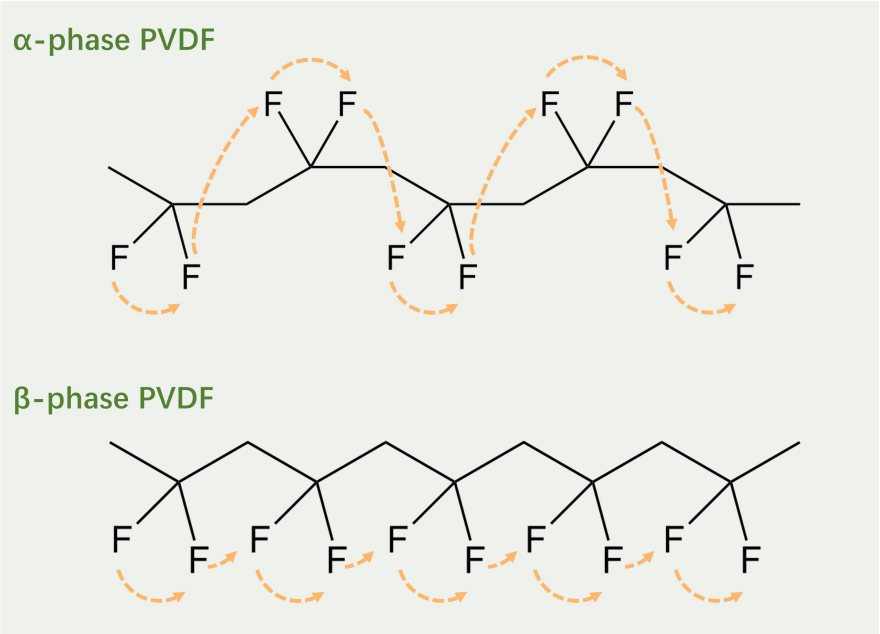

Figure S18. The schematic illustration of Li^+ transport path in α-phase PVDF (upper) and β-phase PVDF (lower), respectively.

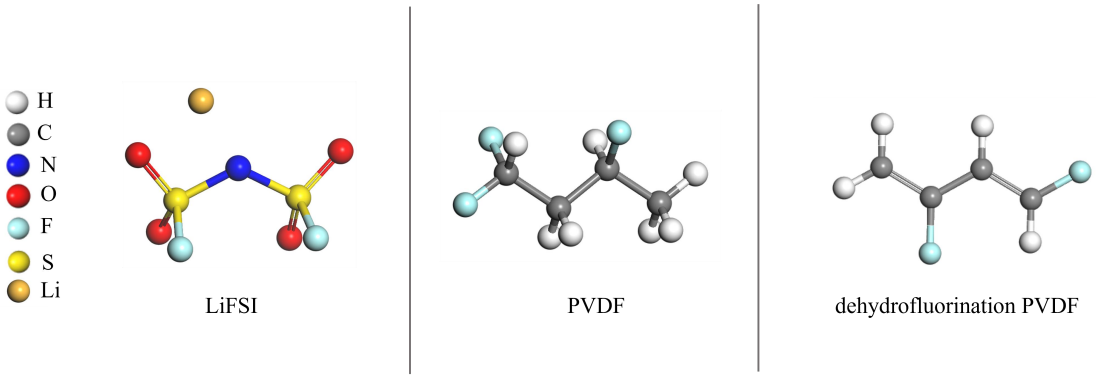

Figure S19. Molecular structure of LiFSI, PVDF and dehydrofluorination PVDF in molecular dynamics.

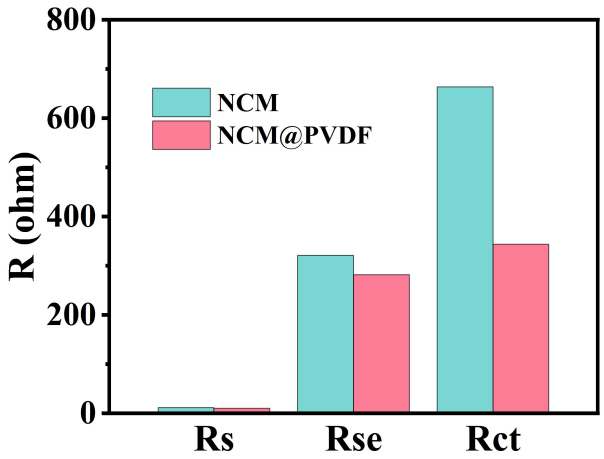

Figure S20. Rs, Rse and Rct results of NCM battery and NCM@PVDF battery fitted from impedance measurement.

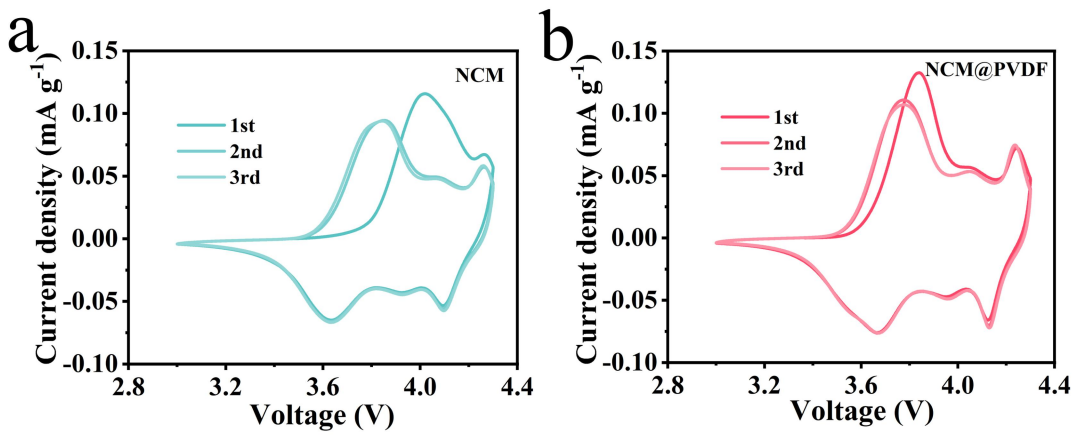

Figure S21. CV curves of (a) NCM battery and (b) NCM@PVDF battery at the scan rate of 0.1 mV s^{-1}.

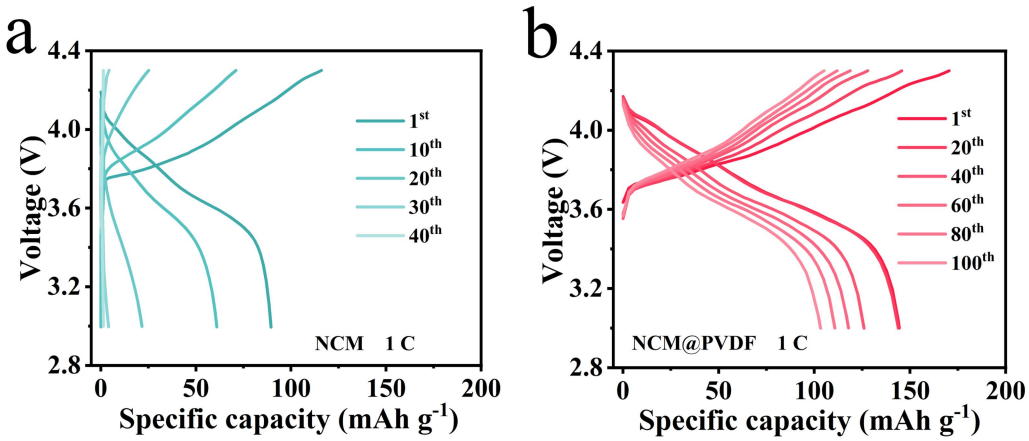

Figure S22. GCD profiles of (a) NCM battery and (b) NCM@PVDF battery.

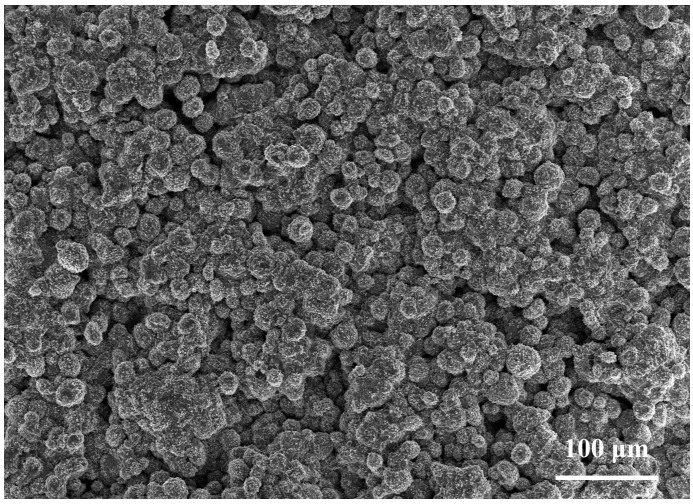

Figure S23. SEM image of the surface of NCM@PVDF cathode after 100 cycles.

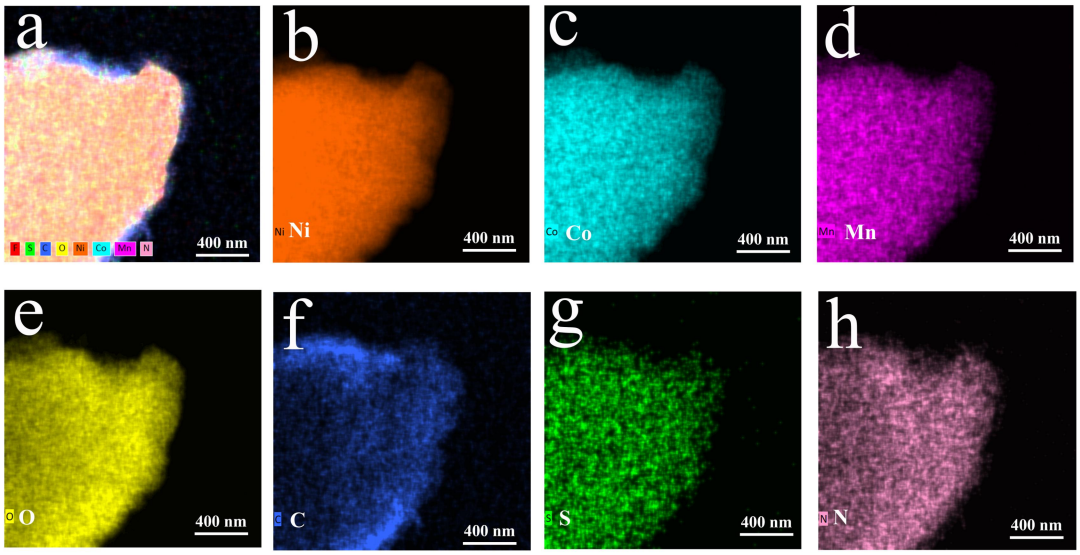

Figure S24. EDS mapping images of NCM@PVDF particle.

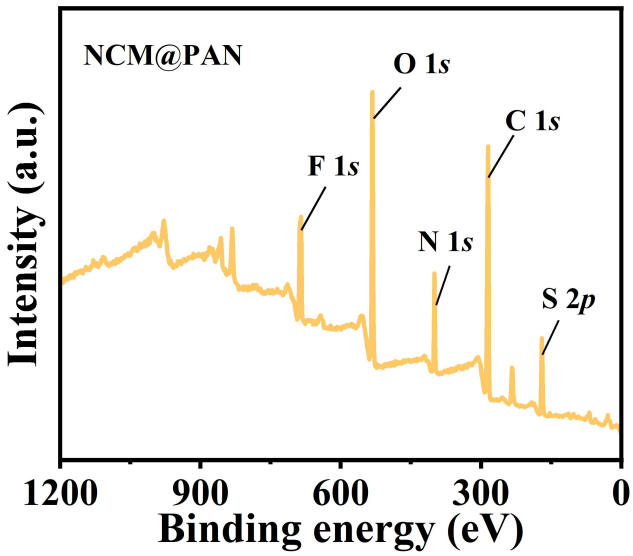

Figure S25. XPS spectrum of NCM@PAN particle.

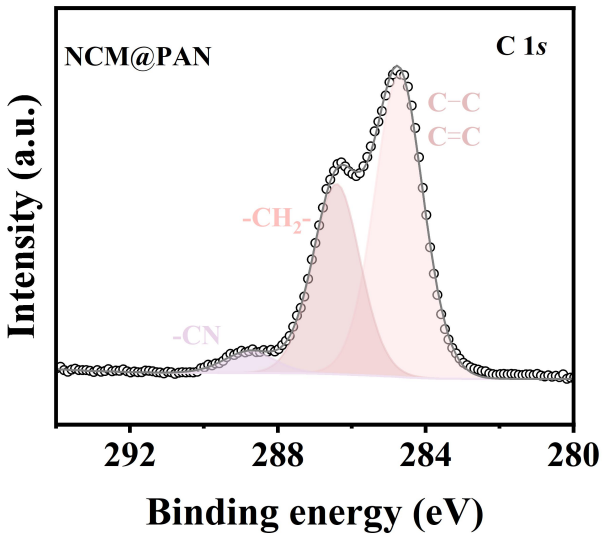

Figure S26. C 1s fine XPS spectrum of NCM@PAN particle.

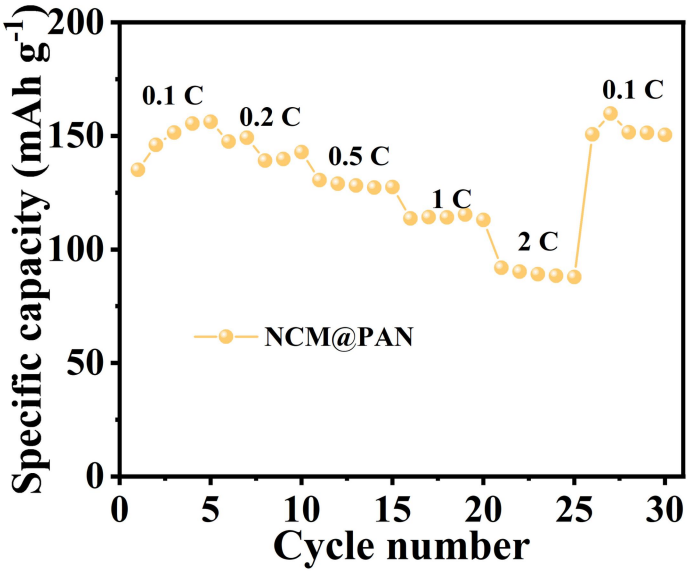

Figure S27. Rate capability of NCM@PAN battery.

Table S1. Pore area and volume of NCM and NCM@PVDF particles.

	Total pore area $m^2 g^{-1}$	Total pore volume $m^3 g^{-1}$
NCM	0.404	0.2829
NCM@PVDF	0.145	0.2793

Table S2. Rs, Rse and Rct results of NCM battery and NCM@PVDF battery fitted from impedance measurement.

	Rs	Rse	Rct
NCM	12.35	176.7	400.6
NCM@PVDF	9.195	99.96	208.9

Table S3. IR drops (V) of NCM battery, NCM@PVDF battery and NCM@PAN battery.

	NCM	NCM@PVDF	NCM@PAN
1st	0.1095	0.1495	0.1287
10th	0.1430	0.1299	0.1203
20th	0.2565	0.1268	0.1166
30th	0.3905	0.1336	0.1274
40th	0.4356	0.1439	0.1411
50th	-	0.1501	0.1544
60th	-	0.1516	0.1550
70th	-	0.1557	0.1674
80th	-	0.1628	0.1817
90th	-	0.1687	0.2025
100th	-	0.1699	0.2366

REFERENCES

1 C. Jiang, Q. Jia, M. Tang, K. Fan, Y. Chen, M. Sun, S. Xu, Y. Wu, C. Zhang, J. Ma, C. Wang and W. Hu, *Angew. Chem. Int. Ed.,* 2021, **60,** 10871-10879.

2 J. Ming, Z. Cao, W. Wahyudi, M. Li, P. Kumar, Y. Wu, J.-Y. Hwang, M.N. Hedhili, L. Cavallo, Y.-K. Sun and L.-J. Li, *ACS Energy Lett.,* 2018, **3,** 335-340.

3 G. Kresse and J. Furthmu¨ller, *Phys. Rev. B,* 1996, **54,** 11169-11186.

4 John P. Perdew, Kieron Burke and M. Ernzerhof, *Phys. Rev. Lett.,* 1996, **77,** 3865-3868.

5 M. Ernzerhof and G.E. Scuseria, *The Journal of Chemical Physics,* 1999, **110,** 5029-5036.

6 D. Choi, J. Kang and B. Han, *Electrochim. Acta,* 2019, **294,** 166-172.

7 S. Grimme, J. Antony, S. Ehrlich and H. Krieg, *The Journal of Chemical Physics,* 2010, **132,** 154104.

8 S. Grimme, S. Ehrlich and L. Goerigk, *J. Comput. Chem.,* 2011, **32,** 1456-1465.

9 K. Momma and F. Izumi, *J. Appl. Crystallogr.,* 2011, **44,** 1272-1276.

10 G. Henkelman, B.P. Uberuaga and H. Jónsson, *The Journal of Chemical Physics,* 2000, **113,** 9901-9904.